AIMS Materials Science, 4(4): 894-904.
DOI: 10.3934/matersci.2017.4.894
Received: 08 June 2017
Accepted: 10 August 2017
Published: 14 August 2017

http://www.aimspress.com/journal/Materials

Research article

First-principles calculation of the electronic and optical properties of $BiRhO_3$ compound

Murat Aycibin * and Naciye ECE

Department of Physics, Faculty of Science, Van Yuzuncu Yil University, 65080 Van, Turkey

*** Correspondence:** Email: murataycibin@yyu.edu.tr.

Abstract: Nowadays, most of the ferroelectric materials have lead element in their formula. Having the lead element as an ingredient is hazardous both human life and environment. For safety reason, we have to replace lead-based compound with lead-free based one. Bismuth-based ferroelectric materials are one of the lead-free ferroelectric compounds. In this paper, we studied $BiRhO_3$ compound belongs to bismuth-based family. We calculated and analyzed $BiRhO_3$ physical properties such as electronic, structural and optical. According to our result, $BiRhO_3$ is classified as a semiconductor with narrow band gap, 0.3 eV, with indirect transition. Moreover, its optical constant depends on choosing axes due to structure type.

Keywords: $BiRhO_3$; electronic structure; lattice constant; density of states; Wien2K

1. Introduction

In 1940s, Hippel et al. and Wul & Goldman discovered ferroelectric behavior in $BaTiO_3$ compounds [1,2]. After discovery of ferroelectric effect in $BaTiO_3$ compound, ferroelectric materials offer a variety of applications in technological areas such as ultrasonic transducers, piezoelectric transformers and acoustic scanners, etc. [3].

Classifying ferroelectric materials according to their structure, we end up with four groups: a) the tungsten-bronze group, b) pyrochlores, c) the bismuth layer-structure group, and d) perovskites. The families, including lead element, represent most of the ferroelectric ceramics manufactured in the world [4]. Unfortunately, the lead-based ferroelectric materials are hazardous for environmental and they need to be replaced with lead-free compounds. The bismuth-based compounds are lead-free compounds [5,6]. In recent years, especially perovskite-type Bi compounds have received more

attention. Researchers have intensively investigated and analyzed bismuth-based compounds due to their extraordinary properties such as lead-free piezoelectric ($BiXO_3$ (X = Al, Sc, Fe, …) and modified version) [7–10], photocatalysts ($BiFeO_3$ and Ga doped version of this compound) [11,12] and multiferroics ($BiXO_3$ (X = Mn, Co, Fe, Cr)) [11–16]. There are some Bi-perovskites compounds ($BiXO_3$ (X = Ti, Cu, Rh, …)) that has been devoted limited studies in literature [17,18].

$BiRhO_3$, having similar electronic analogue to $BiCoO_3$ compound, is one of almost untouched compounds among the $BiXO_3$ (X = Mn, Co, Fe, …) materials [18,19]. In literature, there are limited studies related to $BiRhO_3$ or modified version of compound [18–22]. Due to this reason, information about its structure and dielectric properties is narrow. Therefore, electronic, optical, and structural properties of $BiRhO_3$ are still under cover; hence the compound needs further investigation. The aim of the paper is to obtain electronic, structural and optical properties of $BiRhO_3$ and to give some theoretical information about compound for further investigations.

2. Computational Methods

The calculation described in this paper was performed using Linearized Augmented Plane Wave (LAPW) [23] implemented into Density Functional Theory (DFT). Pseudopotential calculations of total energy, electronic band structure and optical properties were obtained using the WIEN2k packet program [24]. We used 25 hartree for cut-off energy and an appropriate set of k points in chosen grid ($21 \times 29 \times 20$) in the first Brillouin zone (BZ) to compute the density, potential and wave function. Practical applications of DFT require an approximate exchange-correlation energy. To choose the best approximate exchange-correlation energy for true exchange-correlation functional, four different potentials implemented in WIEN2k program were used. These potentials are namely Local Spin Density Approximation (LSDA), Generalized Gradient Approximation (GGA) using the Perdew-Burke-Ernzerhof [25], WC-GGA [26] and PBEsol-GGA [27]. In the calculation, −8.5 Ry energy value was used to separate between valence and core states.

3. Results and Discussion

3.1. Structural Properties

The space group of orthorhombic $BiRhO_3$, non-magnetic material, is Pnma (62). In unit cell, there are 20 atoms. The location of each atom in the unit cell is given in Table 1 and Figure 1. $BiRhO_3$ is perovskite-type compound crystallizing in an orthorhombic system with $a = 5.8089\,Å$ [28], $b = 7.7720\,Å$ [15], $c = 5.3510\,Å$ [28]. The atomic position and space group information about the BiRhO3 compound in unit cell were taken from ref [19]. Atomic electronic configuration of compound is Bi [Xe] $4f^{14}5d^{10}6s^{2}6p^{3}$, Rh [Kr] $4d^{8}5s^{1}$ and O [He] $2s^{2}2p^{4}$. Before starting to calculate physical properties of compound, we implemented the spin-orbit coupling effect on our calculation because 4d electrons have spin-orbit coupling.

As mentioned above, in Wien2k software, there are four type potentials to be used as an exchange-correlation potential. Therefore, we ran volume optimization calculation for each potential to obtain the best theoretical lattice parameters, which are the closest to experimental value and gave the minimum Energy value (Figure 2). For this aim, we used Birch-Murnaghan equation of state [29,30] to fit volume versus energy graph to obtain the theoretical values of the lattice constant

depending on selected potential. All obtained lattice values are inserted in Table 2. In addition, we also obtained bulk modulus, derivative bulk modulus and ground state volume for $BiRhO_3$ and all values were inserted in Table 2.

Table 1. Structure parameters and crystallographic data of $BiRhO_3$ refined in space group 62 (Pnma), Z = 4 at Room Temperature.

Atom	Wyckoff position	Atomic Position		
		x	y	z
Bi	4c	0.06049	1/4	0.98597
Rh	4b	0	0	0.5
O1	4c	0.4687	1/4	0.115
O2	8d	0.3126	0.0431	0.6750

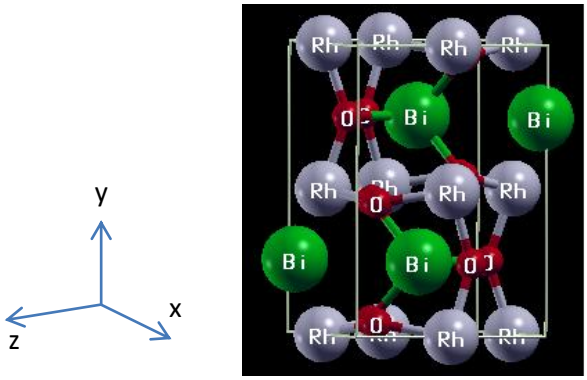

Figure 1. Unit cell of $BiRhO_3$ [30].

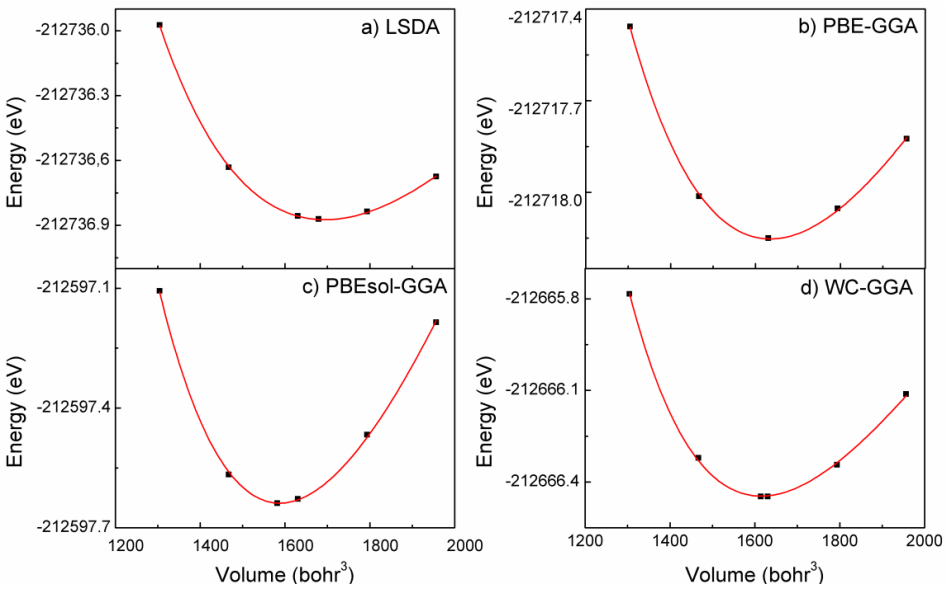

Figure 2. Dependence of total energy versus the unit cell volume by selected potential a) LSDA, b) PBE-GGA, c) PBEsol-GGA and d) WC-GGA for $BiRhO_3$.

Table 2. Calculated ground state volume, lattice constants, bulk modulus, derivative of bulk modulus, ground state energy per unit cell of $BiRhO_3$ depending selected potential.

Lattice Constant	PBE-GGA	LSDA	WC-GGA	PBEsol-GGA	Experimental [19]
a	5.8673	5.751	5.809	5.800	5.8098
b	7.8489	7.694	7.771	7.759	7.7720
c	5.4039	5.297	5.350	5.342	5.3510
Volume ($\mathring{A}^3$)	248.866	234.369	241.612	240.410	241.620
B	182.214	224.027	206.954	201.710	
B'	4.732	4.732	4.732	4.732	

It is clear from Table 2 that WC-GGA potential gives the closet value of the calculated lattice constant to experimental one. After this point, we used the WC-GGA potential for the rest of the calculations instead of exchange-correlation potential. In Figure 3, we also graphed pressure versus volume for four potentials. As seen from Figure 3, zero pressure can be achieved where the minimum volume of the compound was obtained.

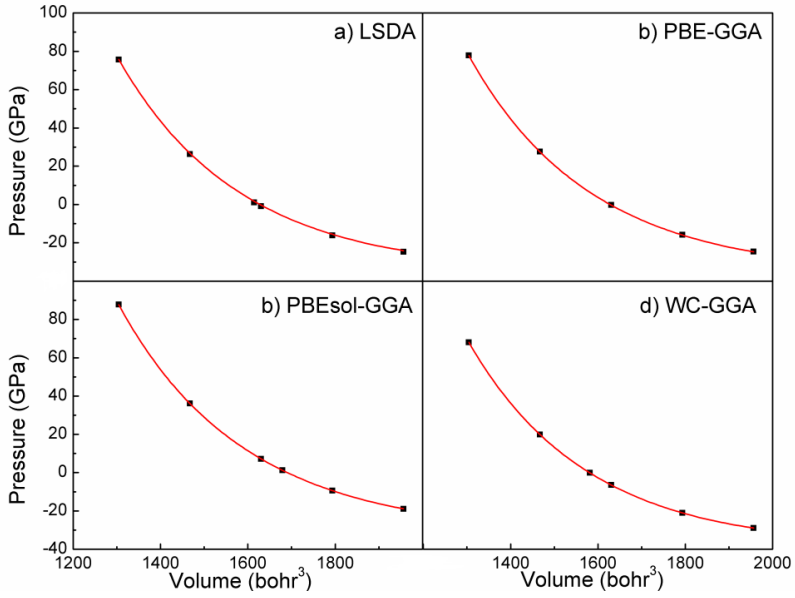

Figure 3. Dependence of pressure versus unit cell volume by selected potential a) LSDA, b) PBE-GGA, c) PBEsol-GGA and d) WC-GGA for $BiRhO_3$.

3.2. Electronic Properties

The calculated band structure of $BiRhO_3$ was given in Figure 4. The Fermi energy level was set to originate. We can see that, there are bands at −17 eV and −11 eV called deep valence band of the compound. To determine forbidden energy bandgap value between the conduction band and valence band to classify compound, y axis was enlarged (Figure 5). As seen from Figure 5, $BiRhO_3$ has an energy band gap 0.302 eV. This result confirms the result of Yi et al. [19]. According to this band

gap value, $BiRhO_3$ compound is classified as a semiconductor. Furthermore, while the top of the valence band is located at X high symmetry point, the bottom of the conduction band is located at Γ high symmetry point in the BZ. As a result, $BiRhO_3$ has indirect transition. This kind of transition includes both photon and phonon for momentum conservation.

Also, we mentioned that we did include the spin-orbit effect to calculation due to the d orbital of Rh element. We also performed without spin-orbit calculation. Comparing these two calculations, we could not see any significant differences.

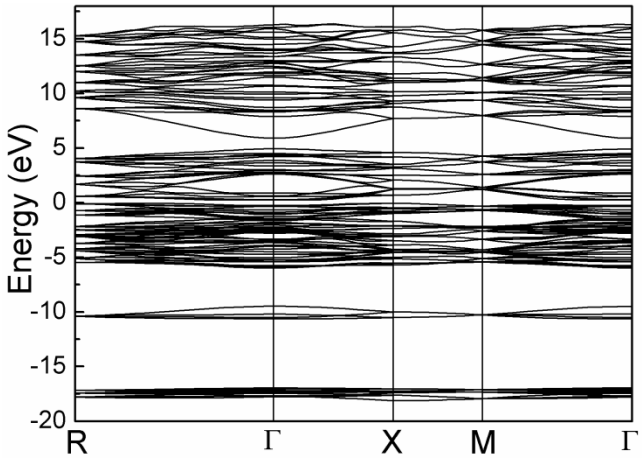

Figure 4. Calculated electronic band structure of $BiRhO_3$.

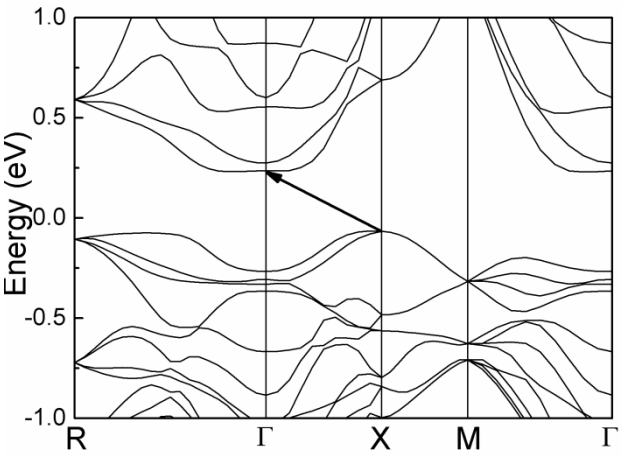

Figure 5. Enlarged version of electronic band structure of $BiRhO_3$.

The electronic density of states (DOS) and the atom resolved partial density of states (PDOS) of $BiRhO_3$ at 0 GPa were also calculated and shown in Figure 6. As seen from Figure 6a, there is a deep valley which is the border line between the bonding state and antibonding states.

All atoms contribute to not only the conduction band, but also the valence band (Figure 6a). This contribution mainly comes from Rh and O atoms comparing with Bi atom. Main contribution to conduction and valence bands comes from Rh atom. Analysing more in detail, the valence band is constructed by Rh-d and O-p orbitals, regardless of where O atoms sit in the unit cell (Figure 6c–d).

The conduction band is mixed by Bi-p, O-p and Rh-d orbitals. Moreover, s orbital of Bi atom contributes to core region.

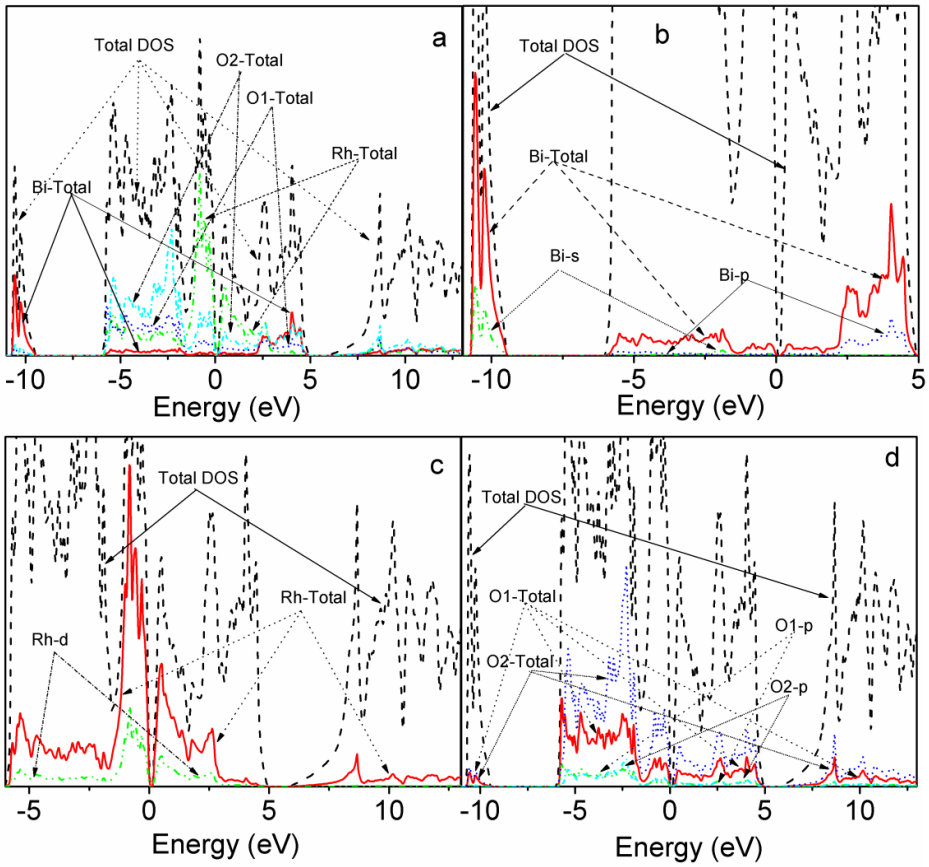

Figure 6. (a) Calculated DOS and PDOS for $BiRhO_3$ crystal, and (b) Partial contribution of Bi, (c) Partial contribution of Rh, (d) Partial contribution of O1 and O2.

3.3. Optical Properties

Next, we will discuss the optical properties of $BiRhO_3$ compound. The linear response of a system due to an external electromagnetic field can be described by the complex dielectric function $\varepsilon(\omega) = \varepsilon_1(\omega) + i\varepsilon_2(\omega)$. In this equation, $\varepsilon_1(\omega)$ and $\varepsilon_2(\omega)$ are real and imaginary parts of the complex dielectric function, respectively. To calculate dielectric function of compound, we have to consider the material structure. Calculating dielectric function, independent from selected axes, are sufficient in cubic crystal structure because $\varepsilon_x(\omega)$, $\varepsilon_y(\omega)$ and $\varepsilon_z(\omega)$ are equal to each other. In contrary, if compound has non-cubic crystal structure, we have to pay attention axes direction to calculate dielectric function.

Since $BiRhO_3$ compound has orthorhombic structure, all dielectric components, dependence on axes, were calculated. The sufficient photon energy range was chosen for the optical response of $BiRhO_3$. The real, $\varepsilon_1(\omega)$, and imaginary part, $\varepsilon_2(\omega)$, of dielectric constant as a function of photon energy were plotted and shown in Figure 7 and Figure 8. We only considered the case of the incident radiation with the linear polarization.

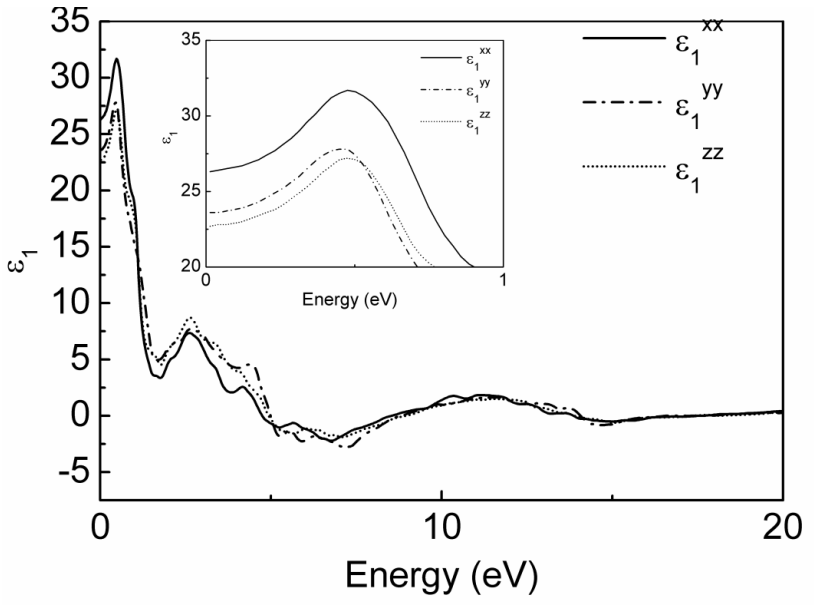

Figure 7. Real part of the dielectric function of $BiRhO_3$ compound depending on chosen axes.

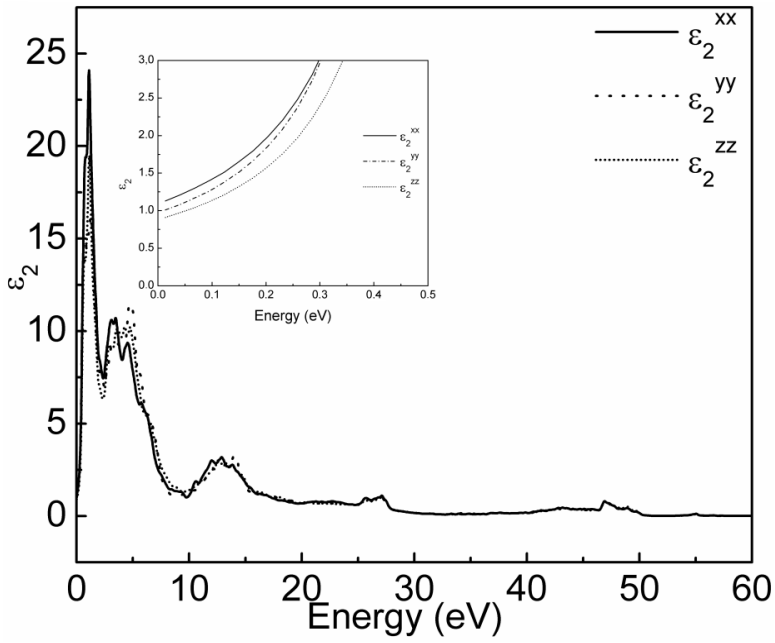

Figure 8. Imaginary part of the dielectric function of $BiRhO_3$ compound depending on chosen axes.

As seen in Figure 7, the static values of the real part of dielectric constant depending on axes, $\varepsilon_1^{xx}(0)$, $\varepsilon_1^{yy}(0)$ and $\varepsilon_1^{zz}(0)$ were found 26.3, 23.6 and 22.7 (small window) , respectively. In addition, $\varepsilon_1(\omega)$ has negative values at the photon energy regions between 4.69–9.075, 13.32–16.04 and 27.36–28.01 eV. In these regions, $\varepsilon_1(\omega)$ has negative value and the incident electromagnetic waves are entirely reflected. There is no transition after 28.01 eV energy values since $\varepsilon_1(\omega)$ gets closer to zero.

The imaginary part of the dielectric function is connected to the energy band structure. Careful analyzing imaginary part of the dielectric function, it was observed that absorption starts before

0.3 eV (small window in Figure 8). In addition, there is a dramatic increase at 0.3 corresponding to the energy band gap where the transition occurs from the valence band to the conduction band. The maximum peak of the imaginary part of dielectric constant located at 1.102 eV is responsible for strong optical transitions.

Figure 9 shows the refractive index according to obtained crystal axes. It is common knowledge refractive index define how light propagates through the material. Due to the structure of the compound, the axes dependence static index of the sample was found as an $n_x(0) = 5.14$, $n_y(0) = 4.86$ and $n_z(0) = 4.77$ (small window).

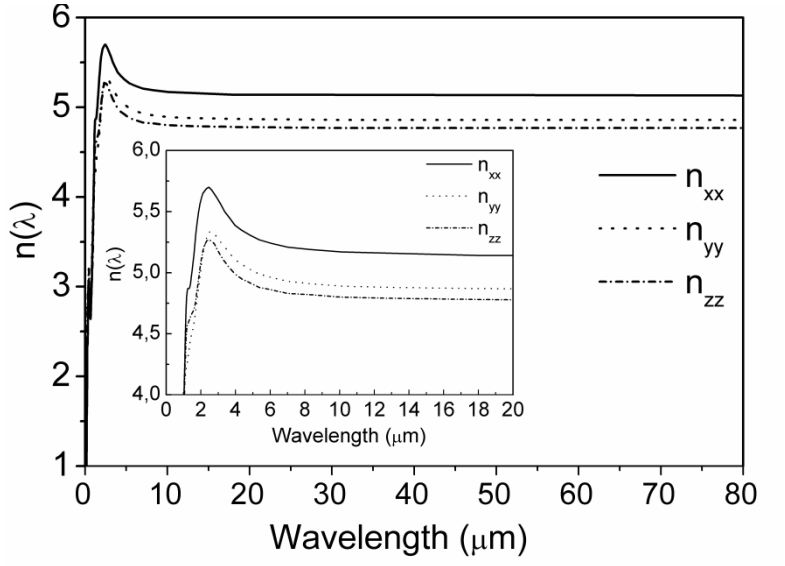

Figure 9. Refraction coefficient of $BiRhO_3$ compound along x, y and z axes.

Finally, Figures 10 and 11 represent three optical constants namely reflectivity R(ω), extinction coefficient k(ω) and energy loss L(ω). They are calculated as functions of incident radiation up to 60 eV. According to our intensive and detailed search, we could not come cross and optical constant of $BiRhO_3$ compound obtained from experimental or other theoretical studies. So they should be understood as a theoretical prediction.

While the reflectivity (Figure 10) is less than 50% for energy range 0 to 3 eV along y and z-axes and more than 50% along the x axis. More than 50% of the incoming electromagnetic beam through 5–10 eV was reflected back at y axis (small window). In this region, photon penetrates through compounds along x and z axes comparing with the y axis.

The local minimum of extinction coefficient k(ω) plot in Figure 11 corresponds to the zero of $\varepsilon_1(\omega)$. The function L(ω) also shown in Figure 11 describes the energy loss of a fast electron traversing the material. It is a well-known fact that the prominent peak in $L(\omega)$ spectra presents the characteristic associated with plasma resonance and corresponding frequency is the so-called plasma frequency ω_p. As seen from Figure 10, sharp peak is associated with plasma oscillation, which correspond negative values of the real part of the dielectric constant. The peak of the L(ω) calculated by the WIEN2k code is located around 28 eV for all axes.

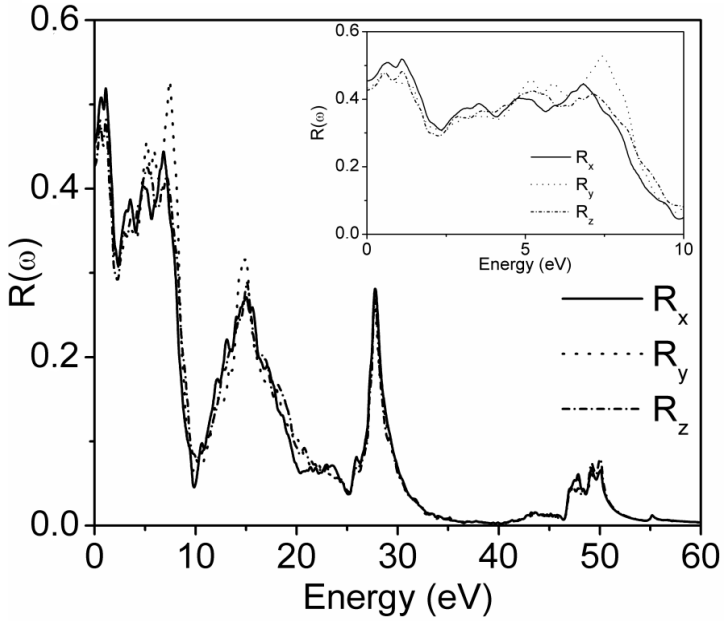

Figure 10. Reflectivity of $BiRhO_3$ compound along x, y and z axes.

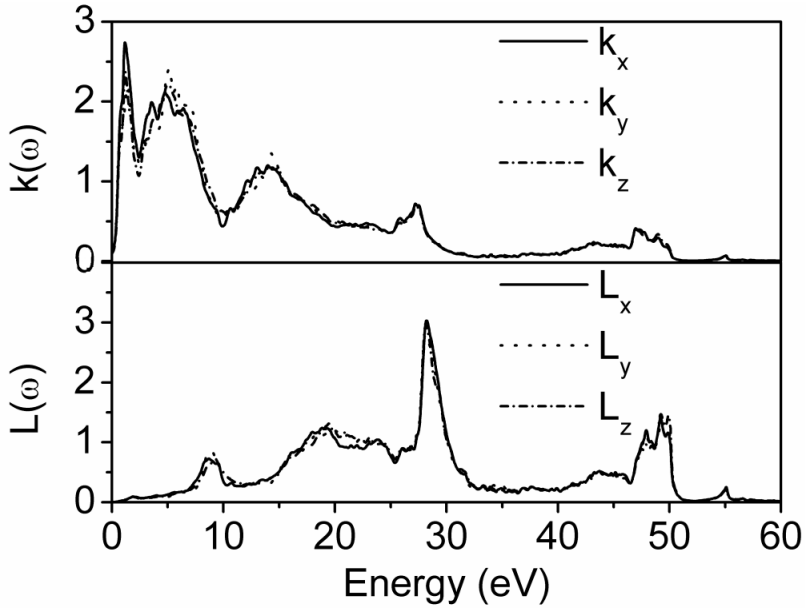

Figure 11. Extinction coefficient and energy loss of $BiRhO_3$ compound along x, y and z axes, respectively.

4. Conclusion

In literature, there are so limited studies related $BiRhO_3$ compound. Hence, we reported electronic, structural and optical properties of $BiRhO_3$. WC-GGA implemented in Wien2K code was used for exchanged and correlation interaction. The obtained relaxed lattice constant is consistent with the experimental result. According to our results, $BiRhO_3$ is a semiconductor and has indirect band gap transition from X to Γ high symmetry point in the Brillioun zone with the value of 0.3 eV.

In addition, we also plot DOS and PDOS. We also calculated energy dependent optical constant of the compound. Unfortunately, we do not come cross with any optical data for compound, so we could not make any comparison.

Acknowledgements

This work was supported by the Unit of Scientific Research Projects of Yuzuncu Yil University under project No. 2015-FED-YL348. The authors also would like to special thanks to Dr. Mustafa TEKPINAR for his critical reading. Also grammer was checked with Gingerly grammer program.

Conflict of Interest

All authors declare no conflicts of interest in this paper.

References

1. Hippel Av, Breckenridge RG, Chesley FG, et al. (1946) High dielectric constant ceramics. *Ind Eng Chem* 38: 1097–1109.
2. Wul B, Goldman JM (1945) Ferroelectric switching in $BaTiO_3$ ceramics. *C R Acad Sci URSS* 51: 21.
3. Ye ZG (2008) *Handbook of Advanced Dielectric, Piezoelectric and Ferroelectric Materials: Synthesis, properties and applications*, Abington Hall, Abington: Woodhead Publishing Limited.
4. Haertling GH (1999) Ferroelectric ceramics: History and technology. *J Am Ceram Soc* 82: 797–818.
5. Izyumskaya N, Alivov Y, Morkoc H (2009) Oxides, Oxides, and More Oxides: High-κ Oxides, Ferroelectrics, Ferromagnetics, and Multiferroics. *Crit Rev Solid State* 34: 89–179.
6. Rodel J, Jo W, Seifert KTP, et al. (2009) Perspective on the Development of Lead-free Piezoceramics. *J Am Ceram Soc* 92: 1153–1177.
7. Baettig P, Schelle CF, LeSar R, et al. (2005) Theoretical prediction of new high-performance lead-free piezoelectrics. *Chem Mater* 17: 1376–1380.
8. Zylberberg J, Belik AA, Takayama-Muromachi E, et al. (2007) Bismuth aluminate $BiAlO_3$: A new lead-free High-T_C piezo-/ferroelectric. 2007 Sixteenth IEEE International Symposium on the Applications of Ferroelectrics, 665–666.
9. Zou TT, Wang XH, Wang H, et al. (2008) Bulk dense fine-grain $(1-x)BiScO_3-xPbTiO_3$ ceramics with high piezoelectric coefficient. *Appl Phys Lett* 93: 192913.
10. Yaakob MK, Taib MFM, Deni MSM, et al. (2013) First principle study on structural, elastic and electronic properties of cubic $BiFeO_3$. *Ceram Int* 39: S283–S286.
11. Wang J, Neaton JB, Zheng H, et al. (2003) Epitaxial $BiFeO_3$ multiferroic thin film heterostructures. *Science* 299: 1719–1722.
12. Catalan G, Scott JF (2009) Physics and Applications of Bismuth Ferrite. *Adv Mater* 21: 2463–2485.
13. Chi ZH, Xiao CJ, Feng SM, et al. (2005) Manifestation of ferroelectromagnetism in multiferroic $BiMnO_3$. *J Appl Phys* 98: 103519.

14. Hill NA, Rabe KM (1999) First-principles investigation of ferromagnetism and ferroelectricity in bismuth manganite. *Phys Rev B* 59: 8759–8769.
15. Belik AA, Iikubo S, Kodama K, et al. (2006) Neutron powder diffraction study on the crystal and magnetic structures of $BiCoO_3$. *Chem Mater* 18: 798–803.
16. Hill NA, Battig P, Daul C (2002) First principles search for multiferroism in $BiCrO_3$. *J Phys Chem B* 106: 3383–3388.
17. Dragomir M, Valant M (2013) Synthesis peculiarities of $BiVO_3$ perovskite. *Ceram Int* 39: 5963–5966.
18. Belik AA (2012) Polar and nonpolar phases of $BiMO_3$: A review. *J Solid State Chem* 195: 32–40.
19. Yi W, Liang QF, Matsushita Y, et al. (2013) Crystal structure and properties of high-pressure-synthesized $BiRhO_3$, $LuRhO_3$, and $NdRhO_3$. *J Solid State Chem* 200: 271–278.
20. Li X, Liu QQ, Han W, et al. (2013) Synthesis and Structural Stability of $BiRhO_3$ at High Pressure. *Int J Mod Phys B* 27: 1362021.
21. Kennedy BJ (1997) Structural trends in Bi containing pyrochlores: The structure of $Bi_2Rh_2O_{7-\delta}$. *Mater Res Bull* 32: 479–483.
22. Longo JM, Raccah PM, Kafalas JA, et al. (1972) Preparation and Structure of a Pyrochlore and Perovskite in the $BiRhO_{3+x}$ System. *Mater Res Bull* 7: 137–146.
23. Andersen OK (1975) Linear methods in band theory. *Phys Rev B* 12: 3060.
24. Blaha P, Schwarz K, Madsen G, et al. (2001) An Augmented Plane Wave Plus Local Orbital Program for Calculating the Crystal Properties, ISBN 3-9501031-1-2.
25. Perdew JP, Burke K, Ernzerhof M (1996) Generalized gradient approximation made simple. *Phys Rev Lett* 77: 3865–3868.
26. Wu ZG, Cohen RE (2006) More accurate generalized gradient approximation for solids. *Phys Rev B* 73: 235116.
27. Perdew JP, Ruzsinszky A, Csonka GI, et al. (2008) Restoring the density-gradient expansion for exchange in solids and surfaces. *Phys Rev Lett* 100: 136406.
28. Oka K, Yamada I, Azuma M, et al. (2008) Magnetic ground-state of perovskite $PbVO_3$ with large tetragonal distortion. *Inorg Chem* 47: 7355–7359.
29. Birch F (1947) Finite Elastic Strain of Cubic Crystals. *Phys Rev* 71: 809–824.
30. Kokalj A (2003) Computer graphics and graphical user interfaces as tools in simulations of matter at the atomic scale. *Comp Mater Sci* 28: 155–168.

AIMS Press